

AN EXPERIMENTAL STUDY OF CRACK DETECTION
IN A ROTATING SHAFT

CENTRE FOR NEWFOUNDLAND STUDIES

**TOTAL OF 10 PAGES ONLY
MAY BE XEROXED**

(Without Author's Permission)

XIAO YINGMING



AN EXPERIMENTAL STUDY OF CRACK DETECTION IN A ROTATING SHAFT

BY

© YINGMING XIAO, B. ENG.

A THESIS SUBMITTED TO THE SCHOOL OF GRADUATE
STUDIES IN PARTIAL FULFILLMENT OF THE
REQUIREMENTS FOR THE DEGREE OF
MASTER OF ENGINEERING

FACULTY OF ENGINEERING AND APPLIED SCIENCE
MEMORIAL UNIVERSITY OF NEWFOUNDLAND

JULY 1995

ST. JOHN'S

NEWFOUNDLAND

CANADA



National Library
of Canada

Acquisitions and
Bibliographic Services

395 Wellington Street
Ottawa ON K1A 0N4
Canada

Bibliothèque nationale
du Canada

Acquisitions et
services bibliographiques

395, rue Wellington
Ottawa ON K1A 0N4
Canada

Your file *Votre référence*

Our file *Notre référence*

The author has granted a non-exclusive licence allowing the National Library of Canada to reproduce, loan, distribute or sell copies of this thesis in microform, paper or electronic formats.

The author retains ownership of the copyright in this thesis. Neither the thesis nor substantial extracts from it may be printed or otherwise reproduced without the author's permission.

L'auteur a accordé une licence non exclusive permettant à la Bibliothèque nationale du Canada de reproduire, prêter, distribuer ou vendre des copies de cette thèse sous la forme de microfiche/film, de reproduction sur papier ou sur format électronique.

L'auteur conserve la propriété du droit d'auteur qui protège cette thèse. Ni la thèse ni des extraits substantiels de celle-ci ne doivent être imprimés ou autrement reproduits sans son autorisation.

0-612-25903-X

Canada

Abstract

This thesis investigated the dynamic characteristics of a rotating shaft by using modal experimental method and an experimental model has been developed for crack detection.

In this study, an imitation crack, which simulates the characteristic of a transverse crack, in the middle span of a rotating shaft, is designed and the rotating shaft experiment setup is made up. Experiments are carried out in different crack parameters and different size rotors in forward and backward rotation.

It is found that the natural frequency of the rotating shaft decreases and frequency response amplitude increases with increasing crack parameter. The maximum difference of natural frequency between cracked and uncracked shaft is 14.7%, and the maximum difference of frequency response amplitude with a crack is 4 times as high as that without crack. It is also found that the rotating shaft in backward rotation has the same vibration response as that in forward rotation.

The experiment results show that the critical speed of the rotating shaft is sensitive to cracks. Therefore, the method may be used in industrial application for detection crack in rotating shafts.

Acknowledgements

The author would like to appreciate the support and encouragement from individuals in the program of Master of Engineering. Particular thanks are due:

(a) Dr. M. R. Haddara, Professor of ocean engineering, for his guidance and financial support throughout this program.

(b) Dr. J. J. Sharp, Dr. Swamidas, Dr. R. Seshadri , Dr. G. Sabin and Dr. L. M. Lye for their courses and help.

(d) Mr. H. Dye, Mr. A. Bursey and other staff in the Machine Shop and Structure Lab. for their technical services and suggestions in manufacturing the setup and processing the experiment.

(e) Finally, his family members, especially his wife, daughter and parents, for their understanding and encouragement.

Contents

Abstract	i
Acknowledgements	ii
Table of Contents	iii
List of Figures	v
List of Tables	vii
List of Symbols	viii
1 Introduction	1
2 Literature Review	3
2.1 Analytical Approach	3
2.2 Experimental Approach	6
2.3 Summary	7
3 Modal Analysis Theory	8
3.1 Analytical Approach	8
3.1.1 Theoretical Method	8
3.1.2 Finite Element Method	21
3.1.3 Finite Element Model of Experimental Setup	31
3.2 Experimental Modal Approach	34
3.2.1 Modal Analysis Theory	34

	iv
3.2.2 Experimental Modal Analysis Methods	40
3.2.3 Modal Data Acquisition	42
3.2.4 Modal Parameter Estimate	46
3.2.5 Modal Data Presentation	47
3.2.6 Summary	47
4 Experimental Study	49
4.1 Experimental setup	49
4.2 Transducer	50
4.3 Instrument	58
4.4 Procedure	63
4.5 Data Analysis	69
4.5.1 Frequency	69
4.5.2 Damping	69
5 Results and Discussion	74
5.1 Static Deflection	74
5.2 Uncracked Shaft	77
5.3 Cracked Shaft	78
5.4 Forward and Backward Rotation	78
5.5 Comparison between Uncracked and Cracked Shaft	78
5.6 Summary	80
6 Conclusion	81
References	88

List of Figures

3.1	(a) Uniform simply supported beam with mass in centre	9
	(b) Uniform simply supported beam	9
	(c) Movement and shear force	10
3.2	Element, node and basic element	24
3.3	Deflection of a shaft	25
3.4	Experimental setup	32
3.5	(a) Simplification of experimental setup	33
	(b) FEM model of experimental setup	33
3.6	Time and frequency domain	38
3.7	Discrete Fourier transform concept	44
4.1	Natural coordinate $y-z$ and rotating coordinate $\eta-\xi$	52
4.2	Simulation crack with variable depth	53
4.3	Principle of the proximity probe in operation	54
4.4	Experimental setup and instrument	61
4.5	Mounted proximity probes	62
4.6	(a) Size of experimental setup	66
	(b) Rotor	67
	(c) Disk and flange	68
4.7	Bandwidth method	70
4.8	Rotation speed and frequency vs amplitude ($c=0$, case 1)	71

4.9	Rotation speed and frequency vs amplitude ($c=0$, case 2)	72
4.10	Amplitude vs relative frequency (case 1)	73
4.11	Amplitude vs relative frequency (case 2)	73
5.1	Vertical deflection vs phase angle	76
5.2	Horizontal deflection vs phase angle	76
5.3	Speed vs amplitude ($c=0.0083$)	83
5.4	Speed vs amplitude ($c=0.1833$)	83
5.5	(a) Speed vs amplitude ($c=0.2041$)	84
	(b) Speed vs amplitude (backward rotation, $c=0.2041$)	84
5.6	Speed vs amplitude ($c=0.3333$)	85
5.7	(a) Speed vs amplitude ($c=0.0083$, case 2)	86
	(b) Speed vs amplitude ($c=0.1833$, case 2)	86
5.8	Speed vs amplitude ($c=0.2041$, case 2)	87
5.9	Speed vs amplitude ($c=0.3333$, case 2)	87
5.10	Comparison of experimental results (case 1)	88
5.11	Comparison of experimental results (case 2)	89
5.12	Natural frequency vs crack parameter	90
5.13	Amplitude vs crack parameter	91

List of Tables

4.1	(a) Characteristics of accelerometer [B&K 4378]	55
	(b) Characteristics of accelerometer [B&K 4379]	56
4.2	Characteristics of proximity probe	57
4.3	List of instrument	60
4.4	Crack parameter	63
5.1	Natural frequency of the shaft system	77
5.2	Results comparison (case 1)	79
5.3	Results comparison (case 2)	80

List of symbols

x, y, z - natural coordinates

γ, η, ξ - rotating coordinates

t - time in seconds

g - gravity acceleration, m/s^2

E - elastic modulus, N/m^2

ρ - mass density, kg/m^3

m - mass, kg/m^2

I_z - moment of inertia about z-axis

A - cross-sectional area, m^2

l - length, m

ω - natural frequency, Hz

ϵ - strain

σ - stress

ξ - damping factor

$[M]$ - $n \times n$ mass matrix

$[C]$ - $n \times n$ damping matrix

$[K]$ - $n \times n$ stiffness matrix

$\{x(t)\}$ - $n \times 1$ vector displacements

$\{f(t)\}$ - $n \times 1$ vector of forces

$h(t)$ - impulse-response function

$H(\omega)$ - frequency response function

$H(s)$ - transfer function

$F(\omega)$ - forcing function

A_{pqr} - residue

A_{pqr}^* - complex conjugate of A_{pqr}

λ_r - system pole

λ_r^* - complex conjugate of λ_r

N - blocksize (power of 2)

T - $N\Delta t$

Δt - time spacing

Δf - frequency spacing

k - $0, 1, 2, \dots, N-1$

f_k - $k\Delta f$

c - crack parameter

d - damping factor

W - thickness of disk

Chapter 1

Introduction

A rotating shaft is an important part in rotating machinery, such as the shaft in a generator. Due to manufacturing flaws or cyclic loading, cracks frequently develop in a rotating shaft. If cracks propagate in the shaft, catastrophic failure will occur. Therefore, we try to detect these cracks as early as possible.

There are different methods to inspect cracks. Modal analysis methods, as one of non-destructive inspection (NDI) methods, has recently become of greater importance. In NDI methods, ultrasonic wave, X-ray, magnetic-particle, permeation and electric potential difference etc. can be used for detecting crack under static condition. The acoustic-emission method (Ivanov, [1984], Simmons et al., [1984] and Grabam et al., [1982]) can be used for inspecting cracks on rotating shafts. Yet a set of specific equipment is needed (Zhao, M. and Luo, Z. H., [1989]). Modal analysis method has the advantages of simplicity in instrumentation and convenience in testing. Thus, the method is widely employed in crack detection in rotating machinery. Modal analysis is defined as the process of characterizing modal parameters (mode shapes, damping factors and frequencies) in a system either through analytical or experimental approach. The

experimental modal approach will be used in the experiment mentioned in this thesis.

Due to cracks, natural frequencies decrease, mode shapes alter depending on the damage magnitude, unit response amplitudes may increase or decrease depending on the position of crack, and damping also changes. By comparing the differences of modal parameters between a cracked and an uncracked structure, we can detect cracks in the tested structure.

The purpose of this study is to carry out experimental modal analysis on the uncracked and cracked rotating shafts supported on elastic bearings and to investigate the relationship between natural frequencies and crack parameter. This study will also provide some useful results for crack detection in industrial applications.

In this study, an experimental setup for simulating a crack in a rotating shaft has been designed. Displacement and acceleration sensors are fixed for collecting vibration responds. Modal parameters were estimated and used to formulate relationships among modal parameters; namely, natural frequencies and damping factors, crack parameters and rotating speed.

Chapter 2

Literature Review

Fatigue cracking in a rotating shaft is one of the main reasons of failure. Crack detection in rotating shafts has received much attention since middle 1970's. Since a crack influences the stiffness of a shaft and the stiffness influences the dynamic behaviour of the shaft, modal analysis or vibration monitoring can be employed to detect crack's initiation and growth.

2.1 Analytical Approach

Kolzow [1974] first pointed out that the vibration monitoring could be useful way in detecting cracks and Shato showed the same idea a little later (Wauer [1990 a]). The work done by Dimarogonas [1970] and Pafelias [1974] introduced the bending stiffness description of a rotor crack which is determined from compliance measurements. The incorporation of the stiffness change caused by a crack into the equation of motion has been dealt with in several papers: Gasch [1976], Henry [1976] , Mayes [1976] and

Dimarogonas [1976].

Gasch [1976] developed a hinge model for Laval rotors which is a simply supported, massless shaft carrying a rigid disk in the middle, in which he replaced the crack mechanism by an additional flexibility and switched it on and off according to whether the crack was closed or open. He discovered that resonances would occur as the rotational speed reached $1/2$, $1/3$, etc., of the shaft bending frequencies.

Henry and Okah-Avae [1976] employed the equations of motion with a shaft section inertia unequal to that of the cracked shaft, and concluded that there would be resonances due to the crack when the rotational speed is equal to $1/n$ of the first critical speed. They also found that the vibration response due to the crack was hardly detectable when the rotational speed exceeded the first critical speed.

Mayes and Davies [1976] performed a detailed analytical investigation of a turbine shaft with cracks. They derived a rough analytical estimation of the crack compliance based on energy principle. Although they considered the non-linear equation for a simple rotor, they obtained analytical solution by considering an open crack which led to a shaft with dissimilar moments of inertia in two perpendicular directions.

Grabowski et al [1982] argued that in a shaft of practical interest the shaft deflection due to its own weight is orders of magnitude greater than the vibration amplitude. Therefore, he suggested that non-linearity does not affect the shaft response since the crack opens and closes regularly with the rotation.

Using the concept that a transverse crack in a structural member introduces local flexibility due to the strain energy concentration in the vicinity of the crack tip under

load, Dimorogonas [1983] and Papadopoulos et al. [1987] derived the complete local flexibility matrix of a cracked, rotating shaft. They observed the local flexibility of the shaft and developed an analytical expression for the effect of the crack on the dynamic response of the rotor.

Dirr and Schmalhorst [1987] described the crack more accurately than others by a 3-dimensional finite element analysis and successfully simulated the vibration of a cracked test rotor on the basis of measured crack shapes.

Qian et al. [1990] derived the element stiffness matrix of a beam with a crack from an integration of stress intensity factors and then established a finite element model of a cracked beam.

Wauer [1990 b] and Collins et al. [1991] developed a beam-like rotating substructure in which, the stiffness and damping properties of a single crack are accurately modelled. They also presented a rotating Timoshenko shaft with a single transverse crack in open and close situation. The governing equation of motion is derived using the principles of fracture mechanics and Galerkin's method. The equations are nonlinear when the crack is open and linear when the crack is closed. When there is a transition from an open crack to a closed crack, or vice versa, some of the stiffness and damping coefficients change.

The analytical approach has advantages for simulating the dynamical behaviour of a cracked and rotating shaft. However, the approach requires enormous amounts of computational time and effort. Furthermore, it is not easy to obtain an accurate measure of the crack effects using an analytical approach. Besides, the validity of the results obtained by the analytical approach can be appropriately assessed only by experimental

study. Therefore, experimental approach has been widely used in the investigation of the addressed problems.

2.2 Experimental Approach

Mayes and Davies [1976] introduced some simplification, especially in relation to time-periodic step function and showed the first experimental results on the dynamics of a cracked shaft.

Ziebarth and Baumgartner [1981] established their crack model on the basis of detailed experimental investigation. They consequently formulated the equations of motion in stationary coordinates and applied them to practical turbine rotors. They, then compared the analytical result with the results of a model test. As practical indicators, they suggested significant peaks in vibration amplitudes, shifting of natural frequencies, unstable vibrations and changes in double-frequency vibration component.

Imam et al. [1988] introduced a Histograms Signature Analysis Technique to reduce the background noise and eliminate the harmonics which exist in an uncracked case. Based on a 3-dimensional finite element crack model and an on-line model, a prototype on-line rotor crack monitoring system was developed and experimentally tested. The system was installed and has been operating on a turbine-generator since 1989.

Wen et al. [1992] tested a simple experimental model system in different crack parameters. He found, that the principal critical speed will decrease with the increase of crack depth and there is unstable region in the vicinity of the principal critical speed. His experimental results are in agreement with that obtained by perturbation and numerical

methods.

Tamura et al. [1988], and Liao and Gasch [1992] built their experimental setup to simulate the crack's opening and closing. Tamur investigated the region of unstable vibration of a rotor with a transverse crack and found that there is an instability near the rotational speed of $2/3$ of critical speed in large crack case. Liao measured accelerations of the system instead of displacements in the super critical speed range.

2.3 Summary

Previous studies reviewed above have investigated the dynamic characteristics of shafts in static and rotational state. Most of these studies have studied the changes in natural frequencies, mode shapes and damping ratios of the shaft due to cracks using analytical method. The study presented in this thesis focuses on the changes of natural frequencies using an experimental method.

Chapter 3

Modal Analysis Theory

Modal analysis is a process of determining modal parameters of a system through analytical or experimental approach. Analytical approach is accomplished by using theoretical method or Finite Element Method (FEM). The modal parameters, such as frequencies and mode shapes can be predicted using these approaches. In the subsequent sections, both methods, theoretical and finite element methods, for modal analytical approach, will be reviewed, then modal experimental approach will be addressed.

3.1 Analytical Approach

3.1.1 Theoretical Method

In this study, a shaft system is simplified as an uniform simply supported beam, with mass in the centre as shown in Figure 3.1a. In order to show the analytical approach simply, at first, we consider only the uniform simply supported beam shown in Figure 3.1b (Shabana, 1990).

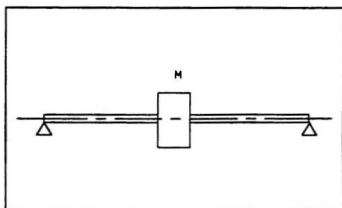


Figure 3.1a: Uniform simply supported beam with mass in centre

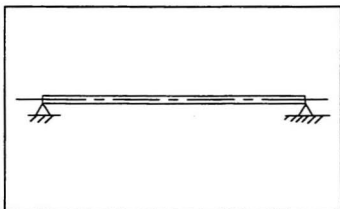


Figure 3.1b: Uniform simply supported beam

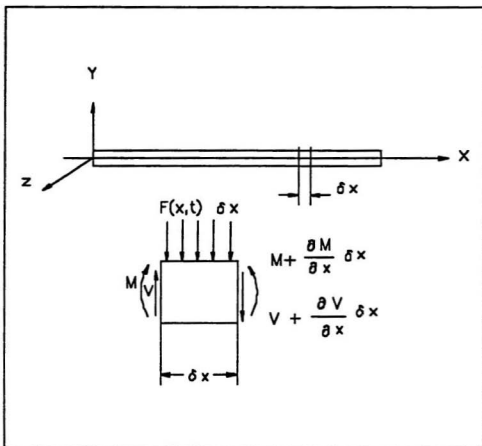


Figure 3.1c: Moments and shear forces

a) Partial Differential Equation

In order to determine the differential equation for the transverse vibration in the shaft or beam. We consider an infinitesimal volume at a distance x from the end of the shaft as shown in Figure 3.1c. The length of this infinitesimal volume is assumed to be δx . Let v , V , M , $F(x,t)$ denotes the transverse displacement of the beam, the shear force, bending moment, and the loading per unit length of the shaft, respectively. Neglecting the rotary inertia, the sum of the moments about the left end of the section yields

$$M + \frac{\partial M}{\partial x} \delta x - M - V \delta x - \frac{\partial V}{\partial x} (\delta x)^2 - F(x,t) \frac{(\delta x)^2}{2} = 0 \quad (3.1)$$

Taking the limit as δx approaches zero, the preceding equation leads to

$$V = \frac{\partial M}{\partial x} \quad (3.2)$$

The dynamic equilibrium condition for the transverse vibration of the shaft is obtained by applying Newton's second law as

$$\rho A \delta x \frac{\partial^2 v}{\partial t^2} = -V - \frac{\partial V}{\partial x} \delta x + V + F(x,t) \delta x \quad (3.3)$$

Equation 3.3 can be rewritten after simplification as

$$\rho A \frac{\partial^2 v}{\partial t^2} = -\frac{\partial V}{\partial x} + F(x,t) \quad (3.4)$$

Substituting Equation 3.2 into Equation 3.4 yields

$$\rho A \frac{\partial^2 v}{\partial t^2} = -\frac{\partial^2 M}{\partial x^2} + F(x,t) \quad (3.5)$$

The moment can be eliminated from this equation by using the moment displacement relationship. To this end, moment, $M = EI_z v''$, is substituted into Equation 3.5. This leads to

$$\rho A \frac{\partial^2 v}{\partial t^2} = -\frac{\partial^2}{\partial x^2} (EI_z v'') + F(x,t) \quad (3.6)$$

If E and I_z are assumed to be constant, Equation 3.6 becomes

$$\rho A \frac{\partial^2 v}{\partial t^2} = -EI_z \frac{\partial^4 v}{\partial x^4} + F(x,t) \quad (3.7)$$

In the case of free vibration, $F(x, t) = 0$ and accordingly

$$\frac{\partial^2 v}{\partial t^2} = -c^2 \frac{\partial^4 v}{\partial x^4} \quad (3.8)$$

where c is a constant defined as

$$c = \sqrt{\frac{EI_z}{\rho A}} \quad (3.9)$$

b) Separation of Variables

Equation 3.8 is a fourth-order partial differential equation that governs the free transverse vibration of the shaft. The solution of this equation can be obtained by using the technique of the separation of variables. In this case, we assume a solution in the form

$$v = \phi(x)q(t) \quad (3.10)$$

where $\phi(x)$ is a space-dependent function, and $q(t)$ is a function that depends only on time. Equation 3.10 leads to

$$\frac{\partial^2 v}{\partial t^2} = \phi(x) \frac{d^2 q(t)}{dt^2} = \phi(x) \ddot{q}(t) \quad (3.11)$$

$$\frac{\partial^4 v}{\partial x^4} = \frac{d^4 \phi(x)}{dx^4} q(t) = \phi^{(4)}(x) q(t) \quad (3.12)$$

Substituting these equation into Equation 3.10, we obtain

$$\phi(x) \ddot{q}(t) = -c^2 \phi^{(4)}(x) q(t) \quad (3.13)$$

which implies that

$$\frac{\ddot{q}(t)}{q(t)} = -c^2 \frac{\phi^{(4)}(x)}{\phi(x)} = -\omega^2 \quad (3.14)$$

where ω is a constant to be determined. Equation 3.14 leads to the following two equations:

$$\ddot{q} + \omega^2 q = 0 \quad (3.15)$$

$$\phi^{iv} - \left(\frac{\omega}{c}\right)^2 \phi = 0 \quad (3.16)$$

The solution of Equation 3.15 is given by

$$q = B_1 \sin \omega t + B_2 \cos \omega t \quad (3.17)$$

For Equation 3.16, we assume a solution in the form

$$\phi = A e^{\lambda x} \quad (3.18)$$

Substituting this assumed solution into Equation 3.16 yields

$$\left[\lambda^4 - \left(\frac{\omega}{c}\right)^2 \right] A e^{\lambda x} = 0$$

or

$$\left[\lambda^4 - \left(\frac{\omega}{c}\right)^2 \right] = 0$$

which can be written as

$$\lambda^4 - \eta^4 = 0 \quad (3.19)$$

where

$$\eta = \sqrt{\frac{\omega}{c}} \quad (3.20)$$

The roots of Equation 3.19 are

$$\lambda_1 = \eta, \quad \lambda_2 = -\eta, \quad \lambda_3 = i\eta, \quad \lambda_4 = -i\eta$$

where $i = \sqrt{-1}$. therefore, the general solution of Equation 3.16 can be written as

$$\phi(x) = A_1 e^{\eta x} + A_2 e^{-\eta x} + A_3 e^{i\eta x} + A_4 e^{-i\eta x} \quad (3.21)$$

which can be rewritten as

$$\phi(x) = A_5 \frac{e^{\eta x} - e^{-\eta x}}{2} + A_6 \frac{e^{\eta x} + e^{-\eta x}}{2} + A_7 (-i) \frac{e^{i\eta x} - e^{-i\eta x}}{2} + A_8 \frac{e^{i\eta x} + e^{-i\eta x}}{2} \quad (3.22)$$

where $A_1 = (A_5 + A_6)/2, \quad A_2 = (A_6 - A_5)/2$

$$A_3 = (A_8 - iA_7)/2, \quad A_4 = (A_8 + iA_7)/2$$

Equation 3.22 can then be rewritten, using Euler's formula of the complex variables,

as

$$\phi(x) = A_5 \sinh \eta x + A_6 \cosh \eta x + A_7 \sin \eta x + A_8 \cos \eta x \quad (3.23)$$

Substituting 3.17 and 3.23 into Equation 3.10 yields

$$v(x) = (A_5 \sinh \eta x + A_6 \cosh \eta x + A_7 \sin \eta x + A_8 \cos \eta x) \times (B_1 \sin \omega t + B_2 \cos \omega t) \quad (3.24)$$

C) Boundary Conditions

The natural frequencies of the shaft, depend on the boundary condition. In the case, the shaft is simply supported at both ends and the boundary conditions are

$$v(0, t) = 0, \quad v''(0, t) = 0$$

$$v(l, t) = 0, \quad v''(l, t) = 0$$

which imply that

$$\phi(0) = 0, \quad \phi''(0) = 0$$

$$\phi(l) = 0, \quad \phi''(l) = 0$$

It is clear that in this case, there are two geometric boundary conditions that specify the displacements at the two ends of the shaft and there are two natural boundary conditions that specify the moments at the ends of the shaft. Substituting these conditions into Equation 3.23 yields

$$A_6 + A_8 = 0, \quad A_6 - A_8 = 0$$

$$A_5 \sinh \eta l + A_6 \cosh \eta l - A_7 \sin \eta l - A_8 \cos \eta l = 0 \quad (3.25)$$

$$A_5 \sinh \eta l + A_6 \cosh \eta l + A_7 \sin \eta l + A_8 \cos \eta l = 0$$

These equations are satisfied if $A_5 = A_6 = A_8 = 0$ and

$$A_7 \sin \eta l = 0 \quad (3.26)$$

The roots of Equation 3.26 are

$$\eta l = n\pi \quad (3.27)$$

where $n=1, 2, 3, \dots$

Therefore, we get the natural frequencies

$$\omega_n = \frac{n^2 \pi^2}{l^2} \sqrt{\frac{EI}{A\rho}} \quad (3.28)$$

and the corresponding models of vibration are

$$\phi_n = A_n \sin \eta_n x \quad (3.29)$$

When $n=1$, we can rewrite Equation (3.29) as

$$\phi = A_0 \sin \frac{\pi x}{l} \quad (3.30)$$

where A_0 is a constant.

The solution for the free vibration of the simply supported shaft can then be written as

$$v(x,t) = \sum_{n=1}^{\infty} \phi_n q_n = \sum_{n=1}^{\infty} (C_n \sin \omega_n t + D_n \cos \omega_n t) \sin \eta_n x \quad (3.31)$$

When a mass is added at the centre of the shaft shown in Figure 3.1a, Rayleigh's method can be used to determine the fundamental natural frequency of the system. The sum of the kinetic energy and strain energy of a model remains constant and equal to the

maximum kinetic energy. Consequently, the conservation of energy leads to

$$T^* = U^* \quad (3.32)$$

where T^* and U^* are, respectively, the maximum kinetic and strain energies.

The strain energy is

$$U^* = \int_0^l \frac{1}{2} \sigma \epsilon dB \quad (3.33)$$

where σ , ϵ , B and l are, respectively, the stress, strain, volume and length of the shaft.

Using Hooke's law, the stress is given

$$\sigma = \epsilon E \quad (3.34)$$

$$\epsilon = -y \frac{\partial^2 \phi(x)}{\partial x^2} \quad (3.35)$$

where $\phi(x)$ is lateral deflection of simply supported shaft shown in Equation (3.30).

Substituting σ and ϵ into Equation (3.33), we have

$$U^* = \frac{E}{2} \int_0^l \left(\frac{\partial^2 \phi(x)}{\partial x^2} \right)^2 dx \int_0^l y^2 dA \quad (3.36)$$

where $I = \int y^2 dA$, A is area of cross section.

Therefore, the strain energy is

$$U^* = \frac{EI}{2} \int_0^l \left(\frac{\partial^2 \phi(x)}{\partial x^2} \right)^2 dx \quad (3.37)$$

The kinetic energy is

$$T^* = T_s + T_m \quad (3.38)$$

where T_s and T_m is, respectively, the kinetic energy of the shaft and i^{th} added mass.

$$T_s = \frac{1}{2} \int_0^l \frac{\rho A}{g} \omega_n^2 \phi^2(x) dx \quad (3.39)$$

where ρ is the mass density.

$$T_m = \frac{1}{2} \sum_{i=1}^n \omega_n^2 m_i \phi^2(x_i) \quad (3.40)$$

where m_i is the i^{th} added mass and $\phi(x_i)$ is the value of the amplitude at the location of mass.

$$T^* = \frac{1}{2} \omega_n^2 \left(\int_0^l \frac{\rho A}{g} \phi^2(x) dx + \sum_{i=1}^n m_i \phi^2(x_i) \right) \quad (3.41)$$

Equating the maximum strain energy to the total maximum kinetic energy of the shaft and added masses, we have

$$\frac{1}{2} \omega_n^2 \int_0^l \frac{\rho A}{g} \phi^2(x) dx + \sum_{i=1}^n m_i \phi^2(x_i) = \frac{EI}{2} \int_0^l \left(\frac{\partial^2 \phi(x)}{\partial x^2} \right)^2 dx \quad (3.42)$$

the equation of frequency becomes

$$\omega_n = \frac{EI \int_0^l [\phi''(x)]^2 dx}{\frac{\rho A}{g} \int_0^l \phi^2(x) dx + \sum_{i=1}^n m_i \phi^2(x)} \quad (3.43)$$

Using Equation (3.30), the terms in Equation (3.43) becomes

$$\int_0^l [\phi''(x)]^2 dx = A_0^2 \left(\frac{\pi}{l}\right)^4 \int_0^l \sin^2 \frac{\pi x}{l} dx = A_0^2 \frac{l}{2} \left(\frac{\pi}{l}\right)^4$$

$$\int_0^l \phi^2(x) dx = A_0^2 \int_0^l \sin^2 \frac{\pi x}{l} dx = A_0^2 \frac{l}{2}$$

Because there is only one mass added in the centre of the shaft in the case, we have

$$\sum_{i=1}^n m_i \phi^2(x) = m A_0^2$$

Substituting these terms, Equation (3.43) becomes

$$\omega_n = \sqrt{\frac{E I A_0^2 \frac{l}{2} \left(\frac{\pi}{l}\right)^4}{\frac{\rho A}{g} A_0^2 l + m A_0^2}} \quad (3.44)$$

$$\omega_n = k \frac{\pi^2}{l^2} \sqrt{\frac{E I}{A \rho}} \quad (3.45)$$

where m_s is shaft's mass, m is added mass and

$$k = \sqrt{\frac{g}{1 + \frac{2m}{m_s}}}$$

3.1.2 Finite Element Method

Generally, the solution of the vibration problems of continuous systems is based on the assumption that the deformation of the system can be described by a set of assumed functions (Bickford, 1990). By using this approach, the vibration of the continuous system which has an infinite number of degrees of freedom is described by a finite number of ordinary differential equations. This approach can be used in the case of geometrical shape structure elements. However, in a large scale system with complex shape structure, difficulties may be encountered in defining the assumed shape function.

In order to solve these problems, Finite Element Method (FEM) has been widely used in the dynamic analysis. In FEM, at first, the structure is divided to relatively small

regions called elements which are rigidly interconnected at selected nodal points. The deformation within each element can then be described by interpolating polynomials. The coefficients of these polynomials are defined in terms of physical coordinates called the element nodal coordinates that describe the displacements and slopes of selected nodal points on the element. Therefore, the displacement of the element can be expressed by using the separation of variables as the product of space-dependent functions and time-dependent nodal coordinates. By using the connectivity between elements, the assumed displacement field can be written in terms of the element shape function and nodal coordinates of the structure or shaft. Using the assumed displacement field, the kinetic and strain energy of each element can be developed, thus defining the finite element mass and stiffness matrix. The energy expressions of the shaft can be obtained by summing the energy expressions of its elements (Shabana, 1990). In the case of determining modal parameters, such as frequencies, when we get the mass and stiffness matrices, it is easy to calculate the natural frequencies by FEM. FEM can be considered to consist of four steps: discretization, interpolation, elemental formulation, and assembly and solution of the finite element equations.

(1) Discretization

This is the first step in the finite element procedure, where the body under examination is divided into elements in such a way that the unknown field variable is adequately represented through the body. The shaft is divided into 11 elements as shown in Figure 3.2.

(2) Interpolation

The finite element method works by assuming a given distribution of the unknown variables through each element. The equations of defining the approximating distribution is called interpolation, and can take any mathematical form. In practice, it is usually polynomials. Polynomials are popular because they are easy to formulate and compute, and in particular their differentiation and integration is straightforward to implement on the computer.

Consider a section of the shaft shown in Figure 3.3. There is no deformation along the shaft axis, and planes normal to the axis before loading remain normal after deformation. The slope of the shaft at any section is given by $\partial v/\partial x$, and the displacement in the x direction is found from

$$u = -y \frac{\partial v}{\partial x} \quad (3.46)$$

Therefore, the bending strain in the shaft is

$$e = \frac{\partial u}{\partial x} = -y \frac{\partial^2 v}{\partial x^2} \quad (3.47)$$

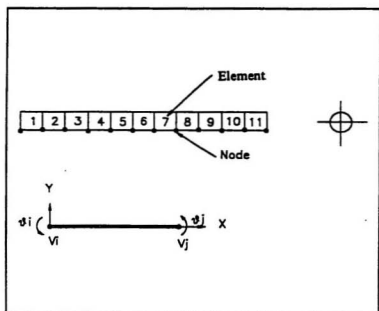


Figure 3.2: Element, node and basic element

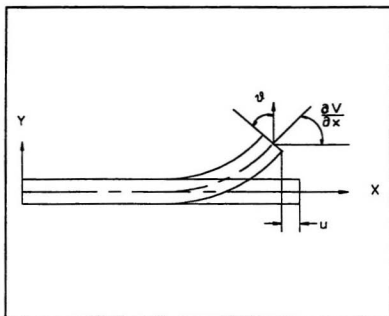


Figure 3.3: Deflection of a shaft

Taking one element shown in Figure 3.2, it is developed with two nodes, and requires a cubic interpolation function for two reasons: Firstly, the element has four boundary conditions (the four degrees of freedom), which demands four coefficients in the approximating function. In addition, however, to ensure that the element satisfies the necessary continuity conditions, that is deflection and slope continuity at the nodes, the interpolation function must be of third order. The function is given by

$$v = a_1 + a_2x + a_3x^2 + a_4x^3 \quad (3.48)$$

and it must satisfy the boundary conditions:

$$\text{at } x = 0, \quad v = v_i \text{ and } \theta = \partial v / \partial x = \theta_i .$$

$$\text{at } x = L, \quad v = v_j \text{ and } \theta = \partial v / \partial x = \theta_j .$$

The resulting four equations can easily be solved to yield

$$a_1 = v_i$$

$$a_2 = \theta$$

$$a_3 = \frac{3(v_j - v_i)}{L^2} - \frac{(2\theta_i + \theta_j)}{L}$$

$$a_4 = \frac{2(v_i - v_j)}{L^3} + \frac{(\theta_i + \theta_j)}{L^2} \quad (3.49)$$

When equations 3.49 are substituted back into the original interpolation function,

equation 3.48 can be rearranged and expressed as

$$v = [N] \{v_i \ \theta_i \ v_j \ \theta_j\} = [N] \{U\} \quad (3.50)$$

(3) Elemental Formulation

By means of the shape function, we can get the element mass and stiffness matrix.

The basic method of finite element formulation is Ritz and Galerkin method. Galerkin method attacks the weak form (weighted Residual) of the differential equation directly and Ritz method uses the energy or functional (calculus of variation) associated with the differential equation as the basis for the development of the finite element model. In this study, Ritz energy method is employed.

The kinetic energy of the element e is defined as

$$A^e = \frac{1}{2} \int_V \rho (v')^2 dV \quad (3.51)$$

where V and ρ are the volume and mass density of the element and

$$v' = [N'] \{U\} \quad (3.52)$$

$$A^e = \frac{1}{2} \{U\}^T \int_V \rho [N'] [N']^T dV \{U\} \quad (3.53)$$

Thus, equation 3.51 can be rewritten as

$$A^e = \frac{1}{2} \{U\}^T [M^e] \{U\} \quad (3.54)$$

Furthermore, we get the element mass matrix.

$$M = \int_V \rho [N]^T [N] dV \quad (3.55)$$

The strain energy is given by

$$T^e = \frac{1}{2} \int \sigma \epsilon dV = \frac{E}{2} \int \epsilon^2 dV \quad (3.56)$$

where $\sigma = E \epsilon$

Substituting equation 3.47 into 3.56, we have

$$T^e = \frac{E}{2} \int_0^l (y''')^2 dx \int y^2 dA \quad (3.57)$$

where $I = \int y^2 dA$, and the strain energy is

$$T = \frac{EI}{2} \int_0^l \left(\frac{\partial^2 v}{\partial x^2} \right)^2 dx \quad (3.58)$$

From equation 3.52 we can get

$$\frac{\partial^2 v}{\partial x^2} = [N'''] \{U\} \quad (3.59)$$

Substituting equation 3.59 into equation 3.58,

$$T^e = \frac{1}{2} \int_0^l (U)^T [K]^e (U)^T dx \quad (3.60)$$

Minimization of the potential energy then gives the now familiar form of the stiffness matrix

$$[K]^e = \int_0^l [N']^T [D] [N'] dx \quad (3.61)$$

where $[D] = E I$

(4) Assembly and Solution of the Finite Element Equations

By using shape function, element nodal coordinates can be transformed natural coordinate system because complex integration can be transformed as simple numerical integration, such as Gauss quadrature which can get a high degree of accuracy for approaching the solution, under the natural coordinate system.

Assembly these element matrix, we have global mass and stiffness matrix

$$[M] = \sum_{e=1}^n [M]^e \quad (3.62)$$

$$[K] = \sum_{e=1}^n [K]^e \quad (3.63)$$

The free undamped vibration is

$$[M]v'' + [K]v = 0 \quad (3.64)$$

As in the case of multi-degree of freedom systems we assume a solution to Equation 3.64 in the form

$$v = B \sin(\omega t + \phi) \quad (3.65)$$

where B is the vector of amplitudes, t is time, ω is the frequency, and ϕ is the phase angle.

Substituting Equation 3.65 into Equation 3.64

$$([K] - \omega^2[M])B = 0 \quad (3.66)$$

For this system of equations to have a nontrivial solution, the determinant of the coefficient matrix must be equal to zero, that is

$$[K] - \omega^2[M] = 0 \quad (3.67)$$

So far, we get the equation 3.67 and know matrix $[K]$ and $[M]$. When the boundary conditions are substituted into the equations, the modal parameters, such as frequencies, can be calculated.

As mentioned earlier, finite element method is an analytical tool which is being used to predict the modal parameters. In the presented study, the general purpose finite element program ABAQUS, Version 5.4, developed by Hibbitt, Karlsson & Sorensen, Inc. is used for analyzing modal parameters.

3.1.3 Finite Element Model of the Experiment Setup

The experiment setup in the study, which will be described detailly in chapter 4, shown in Figure 3.4, consists of a uniform simply supported shaft and a rotor in the centre of the shaft.

The shaft can be described by beam elements in ABAQUS since this is a effective and easy way for FEM analysis, and the rotor can be simplified as a mass in the shaft center. Figure 3.5 illustrates the FEM model of the experiment setup in the study in which the shaft is divided into 11 elements by 23 nodes. According to the model, a program run in ABAQUS is compiled. The result of caculation is compared and shown in chapter 5.

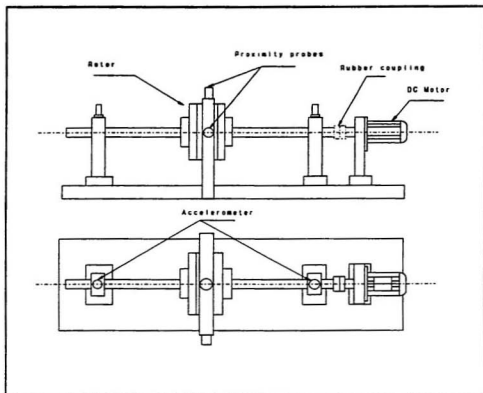


Figure 3.4: Experimental setup

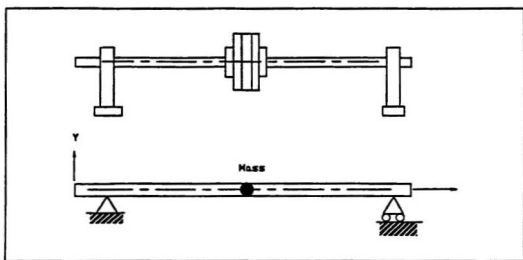


Figure 3.5a: Simplification of experimental setup

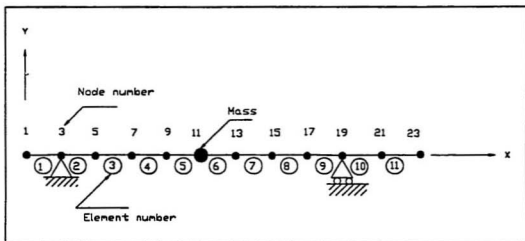


Figure 3.5b: FEM model of experimental setup

3.2 Experimental Modal Approach

Experimental modal approach is the process of determining the modal parameters of a linear, time-invariant system. One of the common reasons of experimental modal approach is to validate the result of the analytical approach. If an analytical model does not exist, the modal parameters determined experimentally serve as the model for future evaluations such as structural modifications. Predominantly, experimental modal approach is used to explain a dynamics problem, vibration or acoustic, that is not obvious from intuition, analytical models, or similar experience (Albert, 1993).

The process of determining modal parameters from experimental data involves the following phases: Modal analysis theory; Experimental modal analysis method; Modal data acquisition and Modal parameter estimation.

3.2.1 Modal Analysis Theory

Modal analysis theory deals with the dynamics of a structure system. But, the system satisfies three assumptions: the first, the system is linear and that its dynamic response can be represented by a series of second order differential equations. The second, the system is time-invariant, which means that the system parameters such as the equivalent mass, stiffness and damping ratio are constants instead of functions of time. The last, the system follows Maxwell-Betti's reciprocal relationships.

Based on the above assumptions, the dynamics of the system is described by transform relationship between different domains, which are time, frequency (Fourier), and Laplace domain. In order to understand modal analysis theory easy, the three domains of a system

are briefly reviewed.

(1) Time Domain (Impulse Response Function)

The general mathematical representation of a single degree of freedom (SDOF) system is expressed

$$M\ddot{x}(t) + C\dot{x}(t) + Kx(t) = f(t) \quad (3.68)$$

where M is the mass .

From differential equation theory, the transient response of the SDOF system to a transient force in form of a theoretical impulse, can be assumed to be in the following form:

$$x(t) = Ae^{\lambda_1 t} + Be^{\lambda_2 t} \quad (3.69)$$

The characteristic frequencies in this solution, λ_1 and λ_2 are determined from the differential equation of Equation 3.68. This yields characteristic frequencies of the following form:

$$\lambda_{1,2} = -\frac{C}{2M} \pm \sqrt{\left[\frac{C}{2M}\right]^2 - \left[\frac{K}{M}\right]} \quad (3.70)$$

The transient response of SDOF can be determined from Equation 3.68, assuming that the initial conditions are zero and that the system excitation $f(t)$ is a unit impulse. The response of the system $x(t)$ to such a unit impulse is known as the impulse-response function $h(t)$ of the system. Therefore:

$$h(t) = A e^{\lambda_1 t} + A^* e^{\lambda_1^* t} \quad (3.71)$$

$$h(t) = e^{\sigma_1 t} [A e^{j\omega_1 t} + A^* e^{-j\omega_1 t}] \quad (3.72)$$

where: σ_1 =damping factor; ω_1 =damped natural frequency.

(2) Frequency Domain (Frequency-Response Function)

Equation 3.68 is the time-domain representation of the system. An equivalent equation of motion may be determined for the Fourier of frequency (ω) domain. This is accomplished by taking the Fourier transform of Equation 3.68. Thus, Equation 3.68 becomes:

$$[-M\omega^2 + jC\omega + K]x(\omega) = F(\omega) \quad (3.73)$$

Equation 3.73 is an equivalent representation of Equation 3.68 in the Fourier domain. If the system forcing function $F(\omega)$ and its response $x(\omega)$ are known, the system characteristic $H(\omega)$ can be calculated. That is the frequency-response function:

$$H(\omega) = \frac{x(\omega)}{F(\omega)} = \frac{1}{-M\omega^2 + jC\omega + K} \quad (3.74)$$

The frequency-response function $H(\omega)$ can be rewritten as a function of the complex poles by using the factored form of the polynomial equation as follows:

$$H(\omega) = \frac{1/M}{(j\omega - \lambda_1)(j\omega - \lambda_1^*)} \quad (3.75)$$

Figure 3.6 is an example to illustrate the domain transformation (from time to frequency domain).

(3) Laplace Domain (Transfer Function)

The equivalent information of equation 3.68 can be presented in the Laplace domain by way of Laplace transform. The only significant difference in the development concerns the fact that Fourier transform is defined from negative infinity to positive infinity while the Laplace transform is defined from zero to positive infinity with initial condition. The development using Laplace transform begins by taking the Laplace transform of equation 3.68. Thus equation 3.68 becomes, assuming zero initial conditions:

$$[Ms^2 + Cs + K]x(s) = F(s) \quad (3.76)$$

Therefore, the transfer function can be defined just as the frequency-response function that was defined earlier.

$$H(s) = \frac{x(s)}{F(s)} = \frac{1}{Ms^2 + Cs + K} \quad (3.77)$$

The quantity $H(s)$ is defined as the transfer function of the system. In other words, a transfer function relates the Laplace transform of the system input to the Laplace transform of the system response. The transfer function can also be written

$$H(s) = \frac{1/M}{s^2 + \left(\frac{C}{M}\right)s + \left(\frac{K}{M}\right)} \quad (3.78)$$

The transfer function $H(s)$ can be rewritten as

$$H(s) = \frac{1/M}{(s - \lambda_1)(s - \lambda_1^*)} \quad (3.79)$$

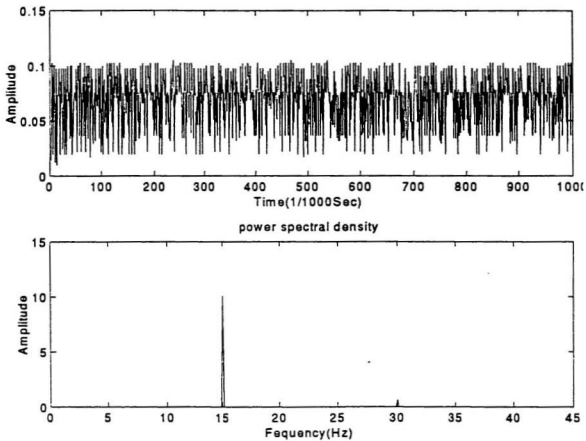


Figure 3.6: Example of domain transformation (case 1, $c=0.10833$ speed=900 rpm)

(4) Transform Relationships of Multi-Degree of Freedom Systems (MDOF)

Just as in the preceding case for SDOF, the equivalent information can be presented for MDOF. The equation of motion for a MDOF system, using matrix notation, is as follows:

$$[M]\ddot{x} + [C]\dot{x} + [K]x = f \quad (3.80)$$

Impulse -response function:

$$H_{pq}(t) = \sum_{r=1}^N A_{pqr} e^{\lambda_r t} + A_{pqr}^* e^{\lambda_r^* t} \quad (3.81)$$

Frequency-response function:

$$H_{pq}(\omega) = \sum_{r=1}^N \frac{A_{pqr}}{j\omega - \lambda_r} + \frac{A_{pqr}^*}{j\omega - \lambda_r^*} \quad (3.82)$$

Transfer function:

$$H_{pq}(s) = \sum_{r=1}^N \frac{A_{pqr}}{s - \lambda_r} + \frac{A_{pqr}^*}{s - \lambda_r^*} \quad (3.83)$$

where

t = time variable

s = Laplace variable

ω = frequency variable

p = measured degree of freedom(response)

q = measured degree of freedom(input)

r = modal vector number

A_{pq} = residue

λ_r = system pole

N = number of modal frequencies

A_{pqr}^* = complex conjugate of A_{pqr}

λ_r^* = complex conjugate of λ_r

3.2.2 Experimental Modal Analysis Methods

There are four general categories of experimental analysis methods: Sinusoidal input-output model; Frequency-response function; Damped complex exponential response and General input-output model (Albert, 1993).

The frequency-response function method is the most commonly used approach for the estimation of modal parameters. This method originated as a testing technique as a result of the use of frequency-response functions in the forced normal mode excitation method to determine natural frequencies and effective number of degrees of freedom. With the advent of the computer, the frequency-response function method became a separate viable technique.

In this method, frequency response functions are measured using excitation at single or multiple points. The relationships between the input F and the responses X or both single and multiple inputs are shown in equations 3.84 through 3.85.

Single-input relationship:

$$X_p = H_{pq} F_q \quad (3.84)$$

$$\begin{Bmatrix} X_1 \\ X_2 \\ \cdot \\ \cdot \\ X_p \end{Bmatrix} = \begin{Bmatrix} H_{1q} \\ \cdot \\ \cdot \\ \cdot \\ H_{pq} \end{Bmatrix} F_q \quad (3.85)$$

Multiple input relationship:

$$\begin{Bmatrix} X_1 \\ X_2 \\ \cdot \\ \cdot \\ X_p \end{Bmatrix}_{N_p \times 1} = \begin{bmatrix} H_{11} & \cdot & \cdot & \cdot & \cdot & \cdot & H_{1q} \\ H_{21} & & & & & & \\ \cdot & & & & & & \\ \cdot & & & & & & \\ H_{p1} & \cdot & \cdot & \cdot & \cdot & \cdot & H_{pq} \end{bmatrix}_{N_p \times N_i} \begin{Bmatrix} F_1 \\ F_2 \\ \cdot \\ \cdot \\ F_q \end{Bmatrix}_{N_i \times 1} \quad (3.86)$$

The frequency-response functions are used as input data to algorithms that estimate modal parameters using a frequency-domain model. Through the use of the fast Fourier transform, the Fourier transform of the frequency-domain mode, the impulse-response function can be calculated for use in modal parameter estimation algorithms involving time-domain models.

Since the Frequency-response Function Method has the advantages mentioned above, the method is used in the experimental study.

3.2.3 Modal Data Acquisition

Acquisition of data deals with the converting of analog signals into a corresponding sequence of digital values that accurately describe the time-varying characteristics of inputs to and responses from a system. In the present study, a Keithley 570 data acquisition system is used. Once the data is available in digital form, the most common approach is to transform it from the time domain to the frequency domain using a fast Fourier transform.

Discrete Fourier Transform

The Discrete Fourier Transform (DFT) is the basis for the formulation of any frequency-domain function in data acquisition systems. In terms of an integral Fourier transform, for a function to be evaluated, it must exist for all time in a continuous sense. For the realistic measurement situation, data are available in discrete sense over a limited period. Figure 3.7 represents the Discrete Fourier Transform (DFT) concept.

Integral Fourier transform :

$$X(f) = \int_{-\infty}^{\infty} x(t) e^{-j2\pi ft} dt \quad (3.87)$$

Inverse Fourier transform :

$$x(t) = \int_{-\infty}^{\infty} X(f) e^{j2\pi ft} df \quad (3.88)$$

Discrete Fourier transform :

$$X(f_k) = \sum_{n=0}^{N-1} x(t_n) e^{-j2\pi f_k t_n} \quad (3.89)$$

$$X(f_k) = \sum_{n=0}^{N-1} x(t_n) e^{-j2\pi (kn/N)} \quad (3.90)$$

Inverse Fourier transform :

$$x(t_n) = \sum_{k=0}^{N-1} X(f_k) e^{-j2\pi (kn/N)} \quad (3.91)$$

where

N = blocksize (power of 2)

$T = N\Delta t$

Δt = time spacing

Δf = frequency spacing $1/T$

$k = 0, 1, 2, \dots, N-1$

$f_k = k\Delta f$

On the basis of DFT, the periodicity and symmetry of the complex factor $e^{-j(2\pi/N)kn}$ can be exploited to increase the efficiency of DFT computations. It is called the Fast Fourier Transform (FFT). The FFT algorithm for computing the DFT of a sequence is the workhorse of digital signal processing (Wovk, 1991). In this study, the data collected by Keithley S570 in digital form, is transferred as frequency-response function by FFT using the computer software MATLAB, version 4.1, which is a technical computing environment for high-performance numeric computation and visualization.

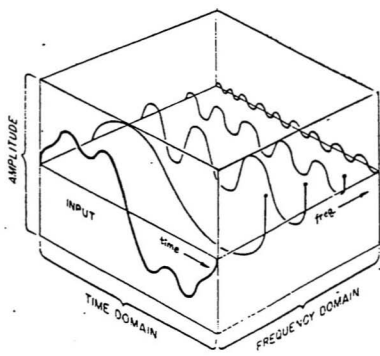


Figure 3.7: Discrete Fourier transform concept

Errors

The accurate measurement of frequency-response function depends on the reduction of errors stemming from the digital signal processing. To take full advantage of experimental data in the evaluation of experimental procedures and verification of theoretical approaches, errors, in measurement, generally designated noise, must be reduced to acceptable levels. The general errors are leakage and aliasing error.

Leakage Error

Leakage error is basically due to a violation of an assumption of the fast Fourier transform algorithm; namely that the true signal is periodic within the sample period used to observe the sample function. When both input and output are totally observable (transient input with completely observed decay output within the sample period) or are harmonic functions of the time period of observation T , there will be no contribution to the bias error due to leakage. Leakage is probably the most common signal-processing error. The effects of leakage can be only reduced, not completely eliminated. The error can be reduced by method of windowing or weighting functions.

Windowing

Windowing is a process of multiplying signals by some sort of weighting function. By applying weight function or a window, leakage error can be reduced. There are many windows, such as Rectangular, Blackman and Hanning in computer software MATLAB. In this study, a Hanning window is used.

Averaging

Averaging also reduces leakage error. It is one very useful feature of FFT spectrum analysis. Averaging is the ability to combine time records (blocks of data) with previous data to smooth out the display. Since vibration data are not usually stable; namely, it is always variable, we use the signal averaging to smooth the spectrum and reduce random signals.

Averaging can be divided into overlap and summation averaging. For periodic monitoring, it is strongly recommended to do summation averaging (Wowk, 1991). Eight to sixteen averaging are all that is necessary to get a stable spectrum. In this study, summation averaging is used to reduce leakage and noise signals.

Aliasing Error

If that frequency components larger than half of the sampling frequency occur in the analog time history, high-frequency signal can form false peaks in the frequency domain. This is called aliasing. This is a byproduct of the digitizing process. The solution of reducing the error is that sampling frequency is two times as high as the maximum natural frequency of the system; Namely, $F_{\text{sampling}} \geq 2 F_{\text{max}}$. In this study, The sampling frequency is 1000(Hz) and the natural frequency is lower than 100(Hz). Therefore, this sampling frequency is high enough to reduce aliasing error and satisfy the requirement of the data acquisition.

3.2.4 Modal Parameters Estimation

Modal parameter estimation is the estimation of natural frequencies, damping factors and mode shapes from the measured data. The measured data can be in relatively raw form

in terms of force and response data in the time or frequency domain, or in a processed form such as frequency-response functions. Modal parameters estimation carried out in this study is based upon the measured data being in the frequency-response function form. The computer software used to perform the estimation is MATLAB (Signal Analysis) Version 4.1.

3.2.5 Modal Data Presentation

Modal parameters data obtained from experiment and predicted by finite element method are presented in tabular and graphical forms. Therefore, the relationship among time, frequency and amplitude versus frequency are shown clearly, and the peak values of frequency response function can be compared under the different crack parameters.

3.2.6 Summary

Modal analysis is the process of characterizing modal parameters using either analytical approach or experimental approach. In this chapter, the theoretical basis of modal analysis methods is reviewed, and experimental analysis methods are discussed. In this study, beam elements provided by software package ABAQUS, 5.4 version, are used to simulate the shaft. In the experimental part of this study, frequency response functions obtained using a software package MATLAB, 4.1 version, is employed to obtain the modal parameters of the rotating shaft system. Other digital signal processing methods are applied in data acquisition in order to eliminate noise signal and errors, such as averaging and windowing.

The result of the analytical study is reported and experimental results are presented in section 5.2. Furthermore, the comparison of modal parameters is given in section 5.5.

Chapter 4

Experimental Study

Experimental study is an important link of modal analysis, and it is a bridge from modal theoretical analysis to industrial applications for crack detection in rotating shafts. Experimental study makes it possible to gain a direct insight into problems whose analytical solution is difficult to obtain.

In this chapter, an imitation crack, which simulates the characteristic of practical transverse crack, is designed and a rotating shaft system having such as crack is made up. In order to measure the vibration signal of the system, transducers and data acquisition instruments are chosen. The general procedures of the experiment is introduced.

4.1 Experiment Setup

A transverse crack opens and closes, which is also called breathing, during rotation in the case of horizontal shaft, because the shaft is deflected by gravity. When the crack

direction in the direction of the gravity direction, say the crack is open, when the crack direction is in the opposite direction of the gravity, the crack is closed shown in Figure 4.1. Except for the both cases mentioned above, there are both open and closed sections continuously varies during the rotation. It is considered that the flexural rigidity of the shaft also varies.

In order to investigate the relationship between modal and crack parameters; namely frequency and crack depth, we need a crack of variable depth that we can open and close on purpose. However, the transverse cracks of shafts in laboratories are generally small because the shafts are generally slender. Also it is difficult to make different crack depth and that errors due to making the crack will influence the crack characteristics.

In this experiment, a large crack is imitated by the rotor shown in Figure 4.2. It is possible to vary the crack depth up to a large value and the shaft can be safely operated in rotation because the crack is not propagated.

The rotor consists of one mass disk, two flanges and one shaft. The two flanges are symmetrically fixed on both sides of the mass disk by eight bolts. If some bolts are removed symmetrically on the both sides, the removed disk section opens and closes with the rotation of the rotor similar to the behaviour of a crack. The shaft is supported by ball bearings and is coupled to a motor by a rubber joint. The experiment setup is shown in Figure 3.4.

4.2 Transducer

A transducer is a device for converting the mechanical motion of vibration into electric

signal. There are three kinds of transducers: displacement, velocity and acceleration.

The most common type of displacement transducer is the proximity probe shown in Figure 4.3, which operates on the eddy current principle. It sets up a high-frequency electric field in the gap between the end of probe and the metal surface that is moving. The proximity probe senses the change in the gap and therefore measures the relative distance, or displacement between the probe tip and the surface. The proximity probe measures relative displacement. Yet, an accelerometer measure absolutely displacement. The most common acceleration transducer is the piezoelectric accelerometer.

In the experiment, accelerometers [B&K 4378 and 4379,] are used. The characteristics of the accelerometers is shown in Table 4.1. The untouched proximity probes [MS type 924-30] are also used . The characteristics of the proximity probes are shown in Table 4.2.

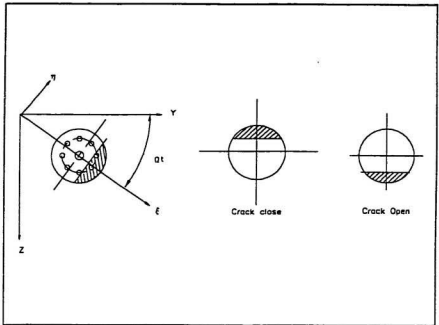


Figure 4.1a: Natural coordinate y - z and rotating coordinate η - ξ

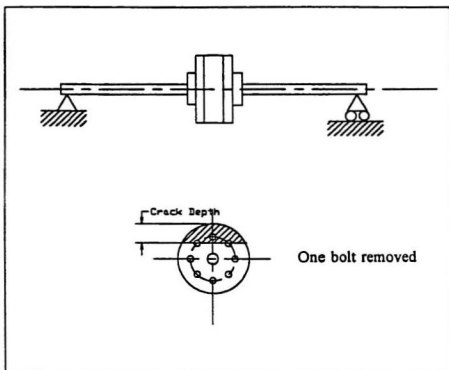


Figure 4.2: Simulation crack with variable depth

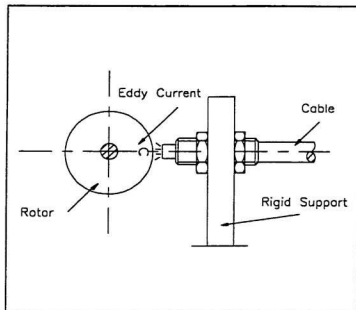


Figure 4.3: Principle of the proximity probe in operation

Table 4.1a: Characteristics of Accelerometer [B&K 4378]

Parameter	Value
Material	Steel AISI 316
Sensing Element	Piezoelectric Material PZ23
Weight	175 gram
Temperature Range	-50 to +250°C
Reference Sensitivity at 159.2 Hz	23°C
Charge Sensitivity	315PC/g
Voltage Sensitivity	258mV/g
Typical Undamped Natural Frequency	13KHz
Capacitance (Incl.cable)	1221 PF
Max.Transverse Sensitivity at 30 Hz	1.4%
Max. Shock Acceleration	20Kms ⁻² peak

Table 4.1b: Characteristics of Accelerometer [B&K 4379]

Parameter	Value
Material	Steel AISI 316
Sensing Element	Piezoelectric Material PZ23
Weight	175 gram
Temperature Range	-50 to +250°C
Reference Sensitivity at 50 Hz	23°C
Charge Sensitivity	310PC/g
Voltage Sensitivity	248mV/g
Typical Undamped Natural Frequency	13KHz
Capacitance (Incl.cable)	1250 PF
Max.Transverse Sensitivity at 30 Hz	0.5%
Max. Shock Acceleration	20Kms ⁻² peak

Table 4.2: Characteristics of Proximity Probe [MS 924-30]

Parameter	Value
Supply Voltage	13.5 to 30VDC
Load Current	12mA max
Output Voltage Range	1 to 9VDC
Output Impedance	50 ohm max
Load Resistance, min	1K to 22 Kohms
Slew Rate	1V/msec
Temperature Drift	$\pm 2\text{mV}^\circ\text{C}/\text{mm}$
Linearity	$\pm 0.25\text{VDC}$ between 1 and 9 VDC
Temperature Range	0 to 60°C
Diameter	30mm
Protection Class	IP67

4.3 Instrument

In this experimental setup shown in Figure 4.4, the DC motor [Eicor 4020-22] drives the shaft for rotation. In order to supply the direct current, 28 voltages and 30 amperes to the motor, a DC power supply made by E&E Lab. of MUN is used. Meanwhile, in order to control the speed of the motor, a DC variable autotransformer is used to adjust the motor's rotational speed. A speed meter [tachmeter 8931] is used to measure the speed. There were 50- 70 rpms differences between measured speed and real speed of rotation. Thus, a stroboscope [IRD 517] is used to measure the speed of rotation. In this case, the difference is only 2-5 rpm between measured and real speed, which is accurate enough for this study. Accelerometers are mounted on the top of bearing housing and proximity probes are fixed near the middle of rotor in horizontal and vertical direction to pick up vibration signal as shown in Figure 4.5. The 15 voltages working volts needed by proximity probes is supplied by DC power supply [Model 1061]. Measured signals are fed to the amplifiers by cables, and amplified by the amplifiers [B&K 2626 and Sundstrand 504E]. After that, the amplified signals are fed to Keithley data acquisition system [KEITHLEY S570] to be converted into a digital signal form. Finally, the vibration signals in digital form are analyzed in Unix computer workstation by using computer software MATLAB 4.1.

In the experimental setup, an oscilloscope [TEKTRONIX 5441] is employed as a signal monitoring.

All of instrument and devices mentioned above are listed in Table 4.3

Table 4.3: List of Instrument

No.	Name of Instrument	Type
1	Proximity Probe	MS Type 924 - 30
2	Accelerometer	B&K Type 4378
3	Accelerometer	B&K Type 4379
4	A/D Converter	Keithley Model 570
5	Storage Oscilloscope	Tektronix Model 5441
6	Amplifier	Soundstrand Type 504E
7	Amplifier	B&K Type 2626
8	Mechanalysis	IRD Model 880
9	Stroboscope	IRD Model 571
10	Tachometer	EMS Type 8931
11	DC Power Supply	Model 1061
12	Autotransformer	Powerstat EM1782
13	DC Motor	Eicor Model 43679
14	Computer	EM Pac Model 486
15	Monitor	Microscan 4G/AD1

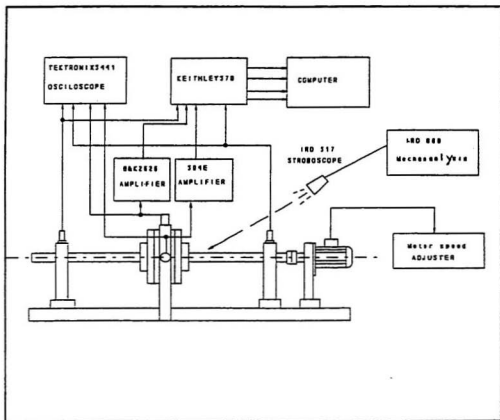


Figure 4.4: Experimental setup and instrument

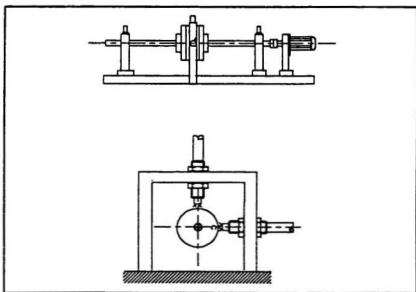


Figure 4.5 Mounted proximity probes

4.4 Procedure

In this experiment, a transverse crack, which opens and closes during rotation, is imitated by removing those bolts connecting the disk and flanges as shown Figure 4.2. One, two, three and four bolts are removed symmetrically from every side of the disk in the experiment, respectively. The crack depth is expressed by crack parameter corresponding to the number of bolts removed. The crack parameter is a non-dimensional parameter. The crack depth due to removing different bolts is divided by the diameter of the disk and the relation between the crack parameter and the number of removed bolts is shown in Table

4.4

Table 4.4: Crack parameter

Removed bolts	Crack parameter (crack depth/ diameter)
0	0
1	0.0833
2	0.1083
3	0.2041
4	0.3333

The procedure of this experiment includes four steps. The first, the static deflection due to the self-weight of the rotor is measured. Secondly, the natural frequency of the static system is measured using a hammer excitation method. Third, the uncracked shaft is tested. Next, the cracked shaft is tested in different crack parameters between 0.083 and 0.333. Finally, the cracked shaft in backward rotation is tested.

The first step is to test static deflection of the rotor. The static deflection of the rotor is measured for the horizontal and vertical direction respectively by proximity probes, shown in Figure 4.5, for one revolution periodic variation from 0° to 360° .

The second step, a single impulse, by hitting the rotor by a rubber hammer, excites the static shaft system to obtain its natural frequency.

The third step, the rotor is driven by a Direct Current (DC) electric motor. Then, the DC is adjusted to reach the speed that we require. At the same time, the stroboscope is tuned on mentioned on chapter 4.2, and aimed the flashlight of strobe at the rotor. After that, the flash rates are changed slightly, once the flash freezes the motion of the rotor, the speed displayed on the readout of the strobe is the speed recorded in the experiment. Since DC is used to change speed of rotation, it have to make sure that speed displayed on readout does not change; namely, the current is stable. Then, the vibration signal is measured by using accelerometers at the speed. After that, direct current is increased by adjusting autotransformer to increase rotating speed, and measure a higher speed than before. The range of tested speed is from 300 rpm to 2000 rpm, which cover the critical speed of the shaft system, since the the motor's power is not high enough over 2000 rpm.

The fourth step, the procedure is the same as the third step. But, we would remove

some bolts and adjust crack parameters before the measurement. The bolts are removed symmetrically on both sides of the disk.

In the experiment, In order to investigate the modal parameter accurately, simulating crack rotor is tested in different sizes, which are $W=58$ (mm) in case 1 ,and $W=90$ (mm) in case 2, shown in Figure 4.6b.

The last step, testin cracked shaft in backward rotation, the procedure is the same as the third step except that the forward rotation is replaced by backward rotation.

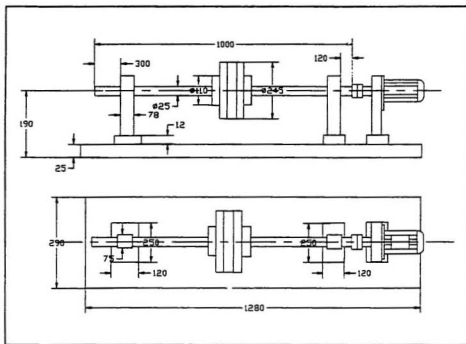


Figure 4.6a: Size of experiment setup (unit: mm)

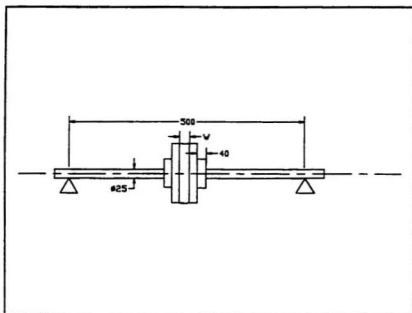


Figure 4.6b: rotor

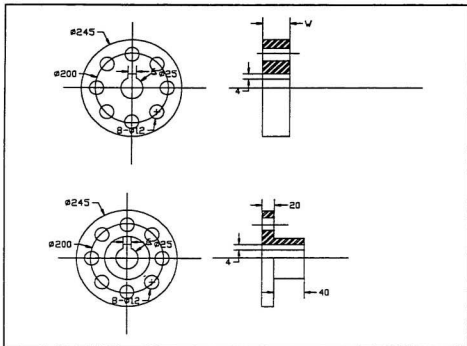


Figure 4.6c: Disk and flange

4.5 Data Analysis

As mentioned before, the vibration response signals from the transducers are converted to a digital form by Keithley S570. After the digital form data is collected, they are sent to Unix computer workstation for further analysis.

4.5.1 Frequency

The data analysis consists of three stages. Firstly, these digital signals are run through a program which averages the data, much of the noise in the signal are removed. Meanwhile, a hanning weight function is used to reduce the leakage error. Then, the vibration response digital signals are transferred from time domain to frequency domain by fast fourier transform which is shown in Figure 3.4. Finally, the measured rotation speed and frequency response amplitude versus the speed are recorded. Repeating the procedure until all those measured signals or data sets at different rotational speed are analyzed, these figures of vibration response amplitude versus these rotational speed and versus the rotational frequencies can be drawn as shown in Figure 4.8 and 4.9. From these graphs, we can find the natural frequency of the shaft system in the experiment setup is 30 Hz in case 1, and 28.33 Hz in case 2.

4.5.2 Damping

Based on these graphs Fig 4.8b and Fig 4.9b, the other graphs, frequency response curves can be developed, by changing the rotational frequency axis to relative rotational

frequency axis Ω/ω (where: Ω is rotation frequency and ω is natural frequency), shown in Figure 4.10 and Figure 4.11.

Taking $r=\Omega/\omega$ as horizontal axis and Amplitude β as vertical axis, bandwidth method (Shabana), one of experimental methods for damping evaluation, can be used to determine damping of the system. Figure 4.7 shows the use of this method in evaluating the damping factor ξ . Using the frequency response curve, we can draw a horizontal line at distance $\beta = (1/\sqrt{2})\beta_{res}$ from the r -axis. This horizontal line intersects the frequency response curve at two points which define the frequencies r_1 and r_2 . The damping factor ξ can be determined by equation: $\xi = (r_2 - r_1)/2$. By means of the bandwidth method, obtain damping factor $\xi = 0.032$ in the case 1, and damping factor $\xi = 0.035$ in case 2 are obtained.

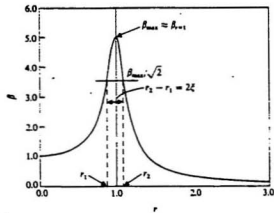


Figure 4.7 Bandwidth method

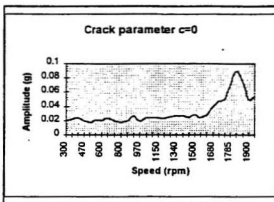


Figure 4.8a: Speed vs amplitude

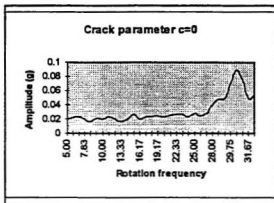


Figure 4.8b: Frequency vs amplitude

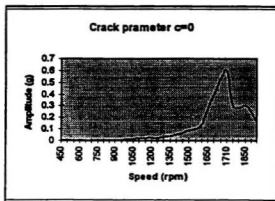


Fig. 4.9a: Speed vs amplitude(case 2)

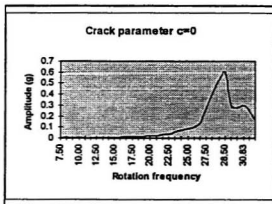


Fig. 4.9b: Frequency vs amplitude (case 2)

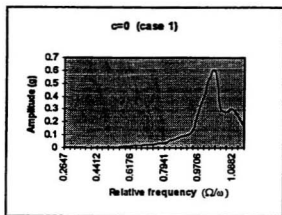


Figure 4.10: Amplitude vs relative frequency (case 1)

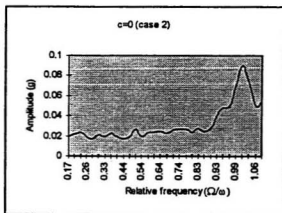


Figure 4.11: Amplitude vs relative frequency (case 2)

Chapter 5

Results and Discussion

In this chapter, firstly, the relationship between static deflection of the rotor and phase angle in vertical and horizontal direction is discussed. Then, the modal parameter, frequency and damping, is considered in the uncracked shaft system. After that, the experiment results dealing with crack parameter are represented. Next, the vibration response of forward and backward rotation of the shaft are shown. Finally, the modal parameters of the system with and without cracks, are compared.

5.1 Static Deflection

The deflection amplitude of the shaft due to self-weight varies with the variation of transverse crack opening and closing in rotation. The static deflection is measured in horizontal and vertical direction respectively. The measured value represents the static deflection of the uncracked and cracked rotor in one revolution periodic variation, which is shown in Figure 5.1. It can be seen that the static deflection increases with increasing

of the crack parameter. In the case of vertical deflection graph, the deflection at phase angle 180° is the largest because of the fully opened crack section, and the deflection at 0° is the smallest due to the fully closed crack section. The result is in agreement with results obtained by Grabowski and Mahrenholtz and Ziebarth et al. (1978.)

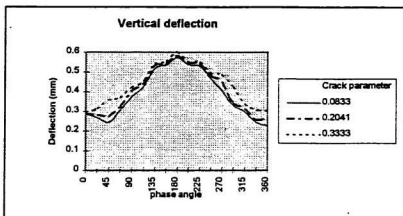


Figure 5.1: Vertical Deflection

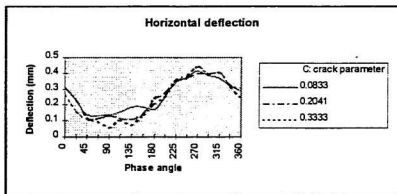


Figure 5.2: Horizontal Deflection

5.2 Uncracked Shaft

In order to determine the natural frequency of the shaft system in the experimental setup, a theoretical calculation, a finite element method approach and a experimental exciting evaluation are applied. The result is shown in Table 5.1.

Table 5.1: Natural frequency of the shaft system

Method	Natural frequency (ω) Hz	
	Case 1	Case 2
Theoretical calculation	32.3	30
FEM calculation	33	31
Exciting evaluation	30.5	28.5
Experimental measurement	30	28.33

Then, all bolts are tightened on the rotor and the vibration response is tested at different rotational speeds. The amplitude versus rotational speed curve is shown in Figure 5.2. It is noted that there is a strong vibration, resonance, at 30 Hz. This means that the natural frequency of the system is 30 Hz. There is a good agreement with the results obtained by other ways mentioned above.

5.3 Cracked Shaft

We measure vibration response at each crack parameter shown in Figure 4.1. The results are shown in Figure 5.3 to 5.5, in case 1, and in Figure 5.6 to 5.9 in case 2. It is found that the larger the crack parameter, the lower the natural frequency is and the bigger the amplitude versus the frequency is.

5.4 Forward and Backward Rotation

Because that there are forward and backward rotating shafts in machinery, the vibration response is measured in both rotational direction, forward and backward. But we find that the response in backward rotation is similar to the forward rotation. Thus, we show only the amplitude versus backward rotational speed curve shown in Figure 5.4b ($c=0.2041$ in case 1).

5.5 Comparison between Uncracked and Cracked Shaft

We show the vibration response of cracked and uncracked shaft system in Figure 4.8 to 5.9, and Table 5.3 and Table 5.4. When we put these figures together, we get Figure 5.10 in case 1, and Figure 5.11 in case 2. As a result, we can compare the experimental results of cracked shaft with that of uncracked shaft. We find that the natural frequency decreases and amplitude versus the frequency increases with increasing crack parameter which are illustrated in Figures 5.12 and 5.13. There are 78% amplitude difference of

between crack parameter 0 and 0.083 and 440% amplitude difference between crack parameter 0 and 0.333 in case 1. Also there are 41% amplitude difference between crack parameters 0 and 0.083 and 147% amplitude difference between crack parameters 0 to 0.333 in case 2. These differences mean that the changes of the modal parameter: the natural frequency, is sensitive to the crack. Therefore, we are able to use modal method to detect the existence of cracks in a rotational shaft.

Table 5.2: Results comparison (case 1)

Crack parameter (c)	Natural frequency ω (Hz)	Amplitude (A)	Amplitude differences ($\Delta A/A_0$)	Frequency differences ($\Delta \omega/\omega_0$)
0	30	0.09	0	0
0.0833	28.83	0.16	0.78	0.039
0.1083	27.5	0.29	2.2	0.083
0.2041	25.83	0.41	3.55	0.139
0.3333	25.08	0.49	4.44	0.146

Table 5.3: Results comparison (case 2)

Crack parameter (c)	Natural frequency ω (Hz)	Amplitude (A)	Amplitude differences ($\Delta A/A_0$)	Frequency differences ($\Delta \omega/\omega_0$)
0	28.33	0.06	0	0
0.0833	27.17	0.125	1.083	0.041
0.1083	26.33	0.14	1.33	0.071
0.2041	24.67	0.16	1.67	0.129
0.3333	24.17	0.17	1.83	0.147

5.6 Summary

The results of static deflection of the shaft system is presented; the natural frequencies obtained by different methods are compared; and the vibration responses having crack or non-crack are shown.

The comparison between cracked and uncracked shaft system shows bigger amplitude difference. Therefore, the difference can be used to distinguish whether or not there are cracks in rotating shaft.

Chapter 6

Conclusion

When there are cracks in a rotating shaft, the modal parameters: the natural frequency and damping will change. This thesis has investigated the relationship between crack parameters and modal parameters by modal experimental method.

In the experimental study, an experimental setup, in which the crack depth is variable, is used to simulate a crack in a rotating shaft. The vibration responses are measured in the range of crack parameter (0 - 0.333).

The conclusions resulted from the experiment are:

1. The shaft system with the variable imitation crack simulates the characteristic of the practical cracked rotors safely and adequately.

2. The shaft deflection is the largest at phase angle 180° in where, the crack is fully opened.

3. The critical speed is sensitive to the crack and the bigger the crack parameter is, the lower the natural frequency is, and the higher the amplitude versus the frequency is.

4. The backward rotation of the shaft has the same frequency response curve as the

forward rotation. Thus, both rotation direction can be chosen in crack detection in rotating shaft.

5. Measuring the acceleration on the rotating shaft by accelerometers is better than measuring shaft deflection when the stiffness of the base of the testing system is not big enough to avoid the relative movement between the testing system and its base.

6. Presented modal experimental method is simple and convenient, and the results obtained by it have a good agreement with that obtained by theoretical and FEM methods. Therefore, it is confirmed that the method is effective for crack detection in rotating shaft.

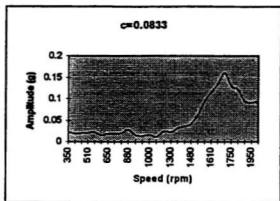


Figure 5.3: Speed vs amplitude ($c=0.0083$)

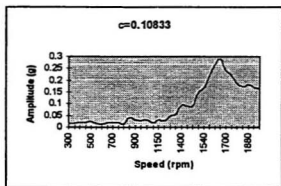


Figure 5.4: Speed vs amplitude ($c=0.1083$)

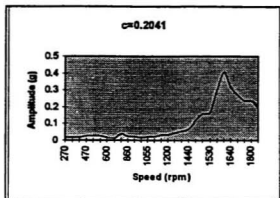


Figure 5.5a: Speed vs amplitude ($c=0.2041$)

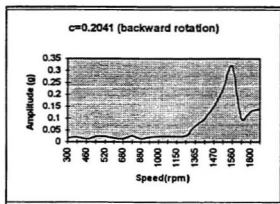


Figure 5.5b: Speed vs amplitude (backward rotation)

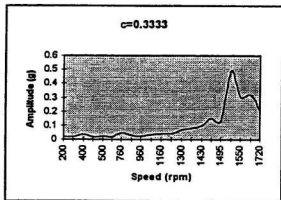
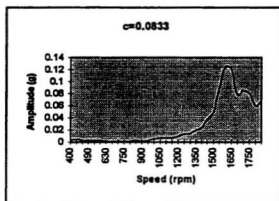
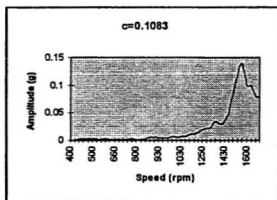
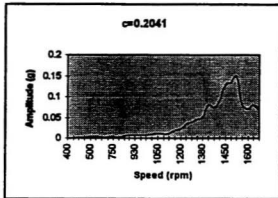
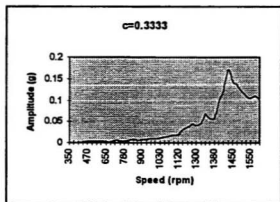


Figure 5.6: Speed vs amplitude ($c=0.3333$)

(Case 2)

Figure 5.7a: Speed vs amplitude ($c=0.0833$)Figure 5.7b: Speed vs amplitude ($c=0.1083$)

(Case 2)

Figure 5.8: Speed vs amplitude ($c=0.2041$)Figure 5.9: Speed vs amplitude ($c=0.3333$)

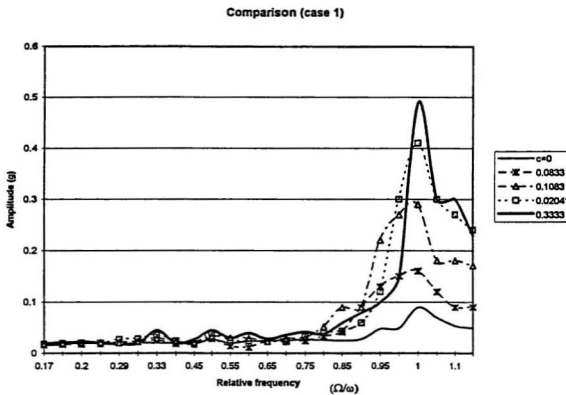


Figure 5.10: Comparison of experimental results (case 1)

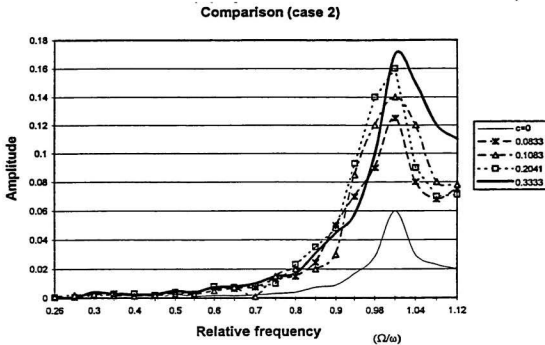


Figure 5.11: Comparison of experimental results (case 2)

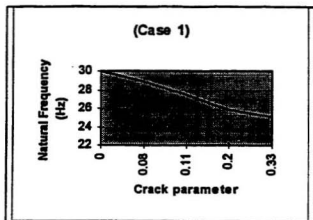


Figure 5.12a: Crack parameter vs natural frequency (case 1)

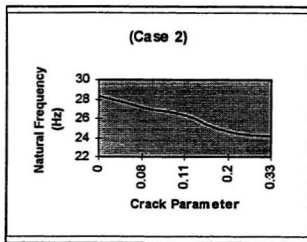


Figure 5.12b: Crack parameter vs natural frequency (case 2)

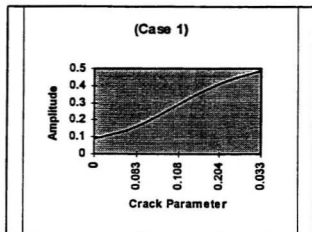


Figure 5.13a: Crack parameter vs amplitude(case 1)

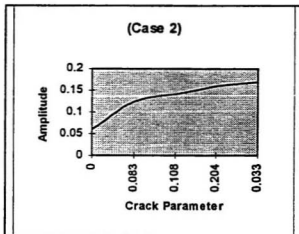


Figure 5.13b: Crack parameter vs Amplitude(case 2)

References

- Albert S. K., 1993, "*Handbook on Experimental Mechanics*" VcH, New York
- Bickford.W.B., 1990 "*A First course in Finite Element Method*" Homewood, Boston
- Cllins, K. R. et al., 1991, "*Detection of Cracks in Rotating Timoshenko Shafts Using Axial Impulses*", Transactions of the ASME, Vol. 113, pp. 74-78
- Dimarogonas, A. D., 1970 "*Dynamic Response of Cracked Rotors*", General Electric Company, Schenectady, NY
- Dimarogonas, A. D. and Papadopoulos, C. A., 1983, "*Vibration of Cracked Shafts in Bending*", J. Sound Vib Vol. 91, pp. 583-593
- Dimarogonas, A. D., 1976, "*Vibration Engineering*", West Publishers, St. Paul
- Dirr, B. O. and Schmalhorsts, B. K., 1987, "*Crack Depth Analysis of a Rotating Shaft by Vibration Measurement*", Rotating Machinery Dynamics, Vol. 2, 11th Biennial Conference on Mechanical Vibration and Noise, Boston, DE Vol. 2, ASME., pp 607-614
- Ewins, D. J., 1984, "*Modal Testing: Theory and Practice*", RSP. London
- Gasch, R., 1976, "*Dynamic Behaviour of a Simple Rotor with a Cross-sectional Crack*", Vibration in Rotating Machinery, Institution of Mechanical Engineer, London, pp.123-128
- Grabowski, B. and Mahrenholtz, O., 1982, "*Theoretical and Experimental Investigations*

of Shaft Vibrations in Turbomachinery Excited by Cracks", Proceedings International Conference on Tordynamic Problems in Power Plants, IFToMM, Rome, pp. 507-514

Grabowski, B., 1980, "*The Vibration behaviour of a Turbine Rotor Containing a Transverse Crack*", J. of Mechanical Design, Vol. 102, pp 140-146

Grabam, L. J. et.al., 1982, "*Acoustic - Emission Monitoring of steam Turbines*", DE82904663

Henry, T. A. and Okah-Avae, B.E., 1976, "*Vibration in Cracked Shaft*", Vibration in Rotating Machinery, Institution of Mechanical Engineer, London, pp.15-19

Imam, I. et al., 1987, "*Development of an On-line rotor Crack Detection and Monitoring System*", Rotating Machinery Dynamics, 11th Biennial Conference on Mechanical Vibration and Noise, Boston, ASME, DE Vol. 2, pp.615-630

Ivanov, V. I., 1984, " Acoustic Emission: Some Problems, Tasks and Solutions", NDT Intl., Vol. 17, No. 6, pp. 323-328

Kolzow, D. R., 1974, "*Abnormal Vibration - A Symptom to Cracked Rotors*", Technical Information Letter, General Electric Company, TIL 727-4 Apr.

Liao, M. and Gasch, R., 1992, "*Crack Detection in Rotating Shafts - an Experimental Study*", Vibration in Rotating Machinery, Institution of Mechanical Engineer, Vol. 432, No. 106, pp. 289-297

Mayes, I. W. and Davies, W. G. R., 1976, "*Dynamic Behaviour of a rotating Shaft System Containing a Transverse Crack*", Vibration in Rotating Machinery, Institution of Mechanical Engineer, London, pp.53-63

Pafelias, T., 1974, "*Dynamic Behaviour of A Cracked Rotor*", Technical Information Series, General Electric Company, No. DF-74-LS-79

Papadopoulos, C. A. and Dimarogonas, A. D., 1987, "Coupled Longitudinal and Bending Vibrations of a Rotating Shaft with an Open Crack", *J of Sound and Vibration* Vol. 147, No. 1, pp. 81-93

Qian, G. L. et al., 1990, "*The Dynamic Behaviour and Crack Detection of a Beam with a Crack*", *J. of Sound and Vibration*, 147 (3), pp. 465-473

Shabana, A. A., 1990, "*Theory of Vibration*", Springer-Verlag, New York

Shatoff, J. 1976 "Using Vibration Analysis to Determine the Dynamic health of Turbine Generators", *Power* 120 (5), pp. 26-28

Simmons, J. A. et al., 1984, "*Theory of Acoustic - Emission from Phase Transformations*" *J. Res. NBS*, Vol. 89, No. 1, pp. 55-64

Smith, J. D., 1989, "*Vibration Measurement & Analysis*", Butterworths, London

Tamura, A. et al., 1988, " *Unstable Vibration of a Rotor with a Transverse Crack*", *Vibration in Rotating Machinery*, Institution of Mechanical Engineer, Vol. 322, No. 88, pp. 467-652

Wauer 1990 (a), "*On the Dynamics of Cracked Rotor - a literature survey*", *Appl. Mech. Rec.*, Vol. 43, No. 1, pp.13-17

Wauer, J., 1990 (b), "*Modelling and Formulation of Equations of Motion for Cracked Rotating Shafts*", *J. Sounds Structures* Vol. 26. No. 8 pp. 901-914

Wen, B. C. and Wang, Y. B., 1988, "*Theoretical Research, Calculation and Experiments of Cracked Shaft Dynamic Response*", *Vibration in Rotating Machinery*, Institution of Mechanical Engineer, Vol. 301, No.88, pp. 473-480

Victor Wowk, 1991, "*Machinery Vibration-Measurement and Analysis*", McGraw-hill, Inc. St. Louis

Ziebarth, H. and Baumgartner, R. J., 1981, "*Early Detection of Cross-sectional Cracks by Turbine Shaft Vibration monitoring Techniques*", ASME Paper 81-JPGC-Pwr-26

Ziebarth, H. et al., 1978, "*Auswirkung von Querrissen auf das Schwingungsverhalten von rotoren*", VDI Berichte, V 320, pp. 37

Zhao, M. and Luo, Z. H., 1989, "*A convenient Method for diagnosis of Shafting Crack*", *Rotating machinery Dynamics*, ASME, Vol. 18, pp. 29-33



